

Journal of Materials Chemistry A

Accepted Manuscript



This is an *Accepted Manuscript*, which has been through the Royal Society of Chemistry peer review process and has been accepted for publication.

Accepted Manuscripts are published online shortly after acceptance, before technical editing, formatting and proof reading. Using this free service, authors can make their results available to the community, in citable form, before we publish the edited article. We will replace this *Accepted Manuscript* with the edited and formatted *Advance Article* as soon as it is available.

You can find more information about *Accepted Manuscripts* in the [Information for Authors](#).

Please note that technical editing may introduce minor changes to the text and/or graphics, which may alter content. The journal's standard [Terms & Conditions](#) and the [Ethical guidelines](#) still apply. In no event shall the Royal Society of Chemistry be held responsible for any errors or omissions in this *Accepted Manuscript* or any consequences arising from the use of any information it contains.



Mechanochemically Synthesized Covalent Organic Framework as Proton-conducting Solid Electrolyte

Received 00th January 20xx,
Accepted 00th January 20xx

DOI: 10.1039/x0xx00000x

www.rsc.org/

Digambar Balaji Shinde,^{a,‡} Harshitha Barike Aiyappa,^{a,b,‡} Mohitosh Bhadra,^{a,b,‡} Bishnu P. Biswal,^{a,b} Prithish Wadge,^a Sharath Kandambeth,^{a,b} Bikash Garai,^{a,b} Tanay Kundu,^{*,a,b} Sreekumar Kurungot^{*,a,b} and Rahul Banerjee^{*,a,b}

Mechanochemistry has become an increasingly important synthetic tool for a waste-free environment. However, the poor quality of the so derived materials in terms of their crystallinity and porosity has been their major drawback for any practical applications. In this report, we have for the first time successfully leveraged such characteristics to show that the mechanochemically synthesized bipyridine based covalent organic framework (COF) outperforms its conventional solvothermal counterpart as an efficient solid-state electrolyte in PEM fuel cells. Marking first of such attempt in COFs, a Membrane Electrode Assembly (MEA) fabricated using the mechanochemically synthesized COFs was observed to inhibit the fuel crossover and build up a stable Open Circuit Voltage (OCV = 0.93 V at 50 °C), thereby establishing itself as an effective solid electrolyte material (with proton conductivity of $1.4 \times 10^{-2} \text{ Scm}^{-1}$), while the solvothermally synthesized COF proved ineffective under similar conditions.

Introduction

The increasing need of day-to-day chemicals and synthetic materials has led to an alarming rise in the generation of hazardous industrial contaminants. Hence, research groups from both academia and industry are attempting to introduce novel routes towards inexpensive, cleaner and competent synthetic protocols for modern day processes.¹ Among all the greener routes, mechanochemistry has gained wide response ever since it has been known to form metal-metal bonds in metallurgic alloys.² Mechano-synthesis involves usage of minimal amount of solvents, while being time efficient alongside, compared to the other conventional methodologies. In recent years, significant progress has been made in forming co-ordination bonds mechanochemically to synthesize industrially important microporous zeolites.³ Moreover, the mechanochemical approach has been demonstrated in realizing multiple bonding involving metal ions/clusters and linkers to form metal-organic frameworks (MOFs) or open framework structures.⁴ Covalent organic frameworks (COFs) are one such example of ordered open framework solids with two or three dimensional motifs covalently linked with C, Si, B, N, O and H.⁵ The embedded porosity and crystallinity in COFs enable a number of applications such as gas adsorption, catalysis, semiconductor

substrate, charge carrier mobility, photoconductivity sensing and super-capacitor.⁶ Such materials could be also rendered functionality under instances wherein the frameworks are devoid of any proton carriers (as in the present case), for the easy impregnation of proton carriers yet strong acids like phosphoric acid. These frameworks were found to retain their chemical stability up to 12M H₃PO₄ loading wherein most of the MOFs fail to withstand such chemical stress. Moreover, unlike most of the MOFs, COFs are light weight, metal-free frameworks with extremely robust chemical as well thermally stable architecture. This helps in easy tuning of such frameworks with desirable functionalities especially towards proton conduction. However, unlike conventional MOF synthesis which can be realized using easy scalable methods *viz.*, solvothermal, microwave, simple mixing, spray drying methods etc.,⁷ the COF synthesis still remains a challenge as it demands the use of vacuum sealed tube technique and extended reaction time, apart from usage of copious amount of solvents for its synthesis. As a result, there is an imperative need for a simpler, faster and neater pathway of COF synthesis from the perspective of both energy and environment. Although, discrete instances of covalent bond formation in zero dimensional organic cages^{8a,b} and polymers^{8c} have been documented, construction of multiple covalent bonds to realize ordered COFs using mechanical energy is far less explored.^{8d} Such mechanochemical method, in contrast to the solvothermal route, could be cost-effective, time-efficient and exclude large amount of harmful solvents. However, COFs synthesized in this way suffer from poor crystallinity and porosity compared to their solvothermal counterparts.⁹ Although mechanochemically synthesised COFs behave closely

^a Physical/Materials Chemistry Division, CSIR-National Chemical Laboratory, Dr. Homi Bhabha Road, Pune-411008, India.

^b Academy of Scientific and Innovative Research (AcSIR), New Delhi, India.

[‡]D.B.S., H.B.A and M. B. contributed equally.

Electronic Supplementary Information (ESI) available: [Synthetic procedures, PXRD, Gas Adsorption, FT-IR, ¹³C solid state NMR, TGA, SEM,TEM, crystallographic data (CIF)]. See DOI: 10.1039/x0xx00000x

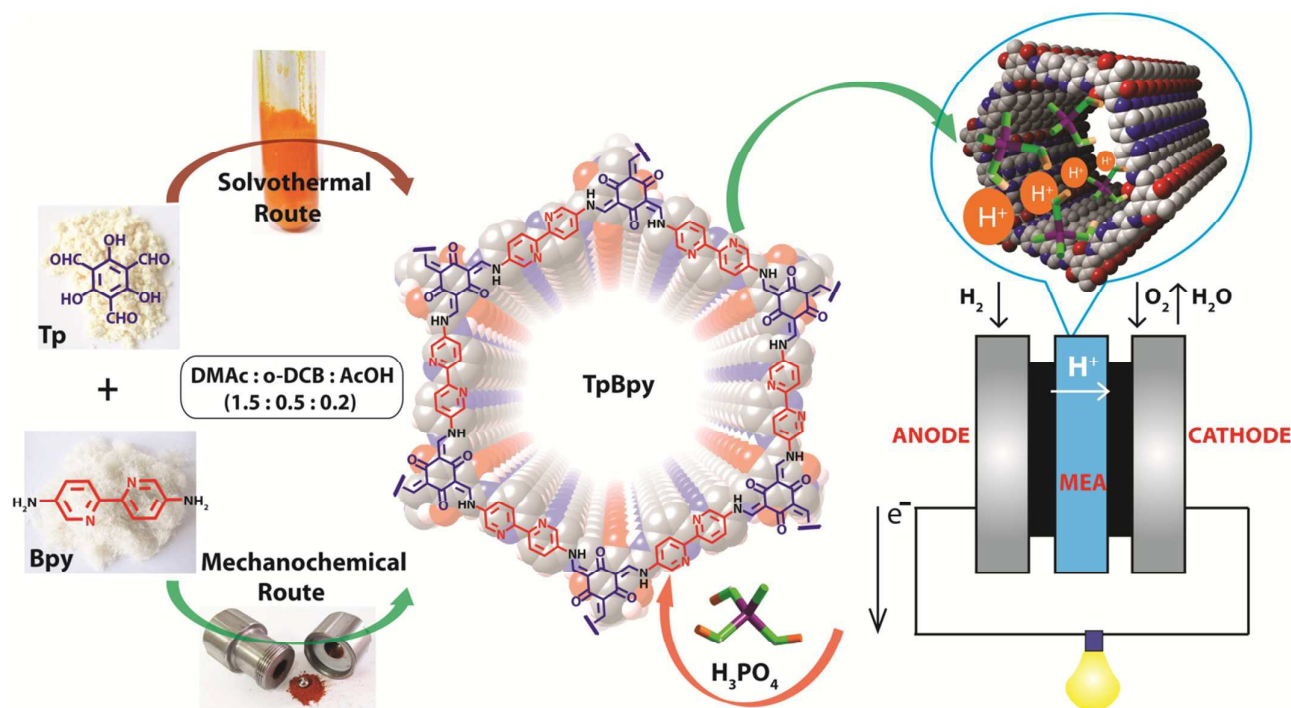


Figure 1. Schematic representation of the synthesis of **TpBpy** COF [via mechanochemical (MC) as well as solvothermal (ST) route] which upon loading of phosphoric acid (PA) forms **PA@TpBpy** and is later integrated as solid electrolyte in PEMFCs.

to that of the cross linked polymer, it is equally imperative to note that unlike the polymers, these COFs have comparatively lower density with similar thermal and chemical stability. Structurally, the COFs are crystalline while polymers are largely amorphous in nature. The amorphous nature of the polymer matrix and their wide pore-size-distribution often result into undefined irregular channels which lengthens the free mean path needed for the transport of protons to a considerable extent. In contrast, the COFs being crystalline have definite pore size distribution and possess periodic channels that promote the easy diffusion of protons. Moreover, these COFs are synthesised using a sustainable, adoptable, energy efficient and scalable mechanochemical route, which involves utilization of minimal amount of solvent. But owing to their poor porosity and low surface area, till date, the solvothermal route has always been preferred over the mechanochemical one to synthesize COFs for practical applications.

Herein, for the first time, we have demonstrated the usefulness of mechanochemically synthesized COF which outperforms its solvothermal counterpart when used under real Proton Exchange Membrane Fuel Cell (PEMFC) operating conditions. We report a bipyridine functionalized COF synthesized via both solvothermal (**TpBpy-ST**) and mechanochemical routes (**TpBpy-MC**) by combining 1,3,5-triformylphloroglucinol (**Tp**) and 2,2'-bipyridine-5,5'-diamine (**Bpy**) through the Schiff base reaction (Figure 1). **TpBpy-MC** exhibits lower crystallinity and porosity compared to **TpBpy-ST** COFs. A recent demonstration of the proton conducting ability of along with the presence of multiple proton binding bipyridine sites in the **TpBpy-ST** and **TpBpy-MC** COFs

motivated us to test their proton conducting ability and evaluate their potential as a solid-state electrolyte in PEMFCs. Although, considerable proton conducting MOFs are reported in the literature,¹⁰ strikingly, till date, there exists only one instance of a proton conducting COF.¹¹ However, its effectiveness as solid-state electrolyte separator in PEMFCs has not yet been validated. Above all, a direct demonstration of the proton conducting ability of such materials under real fuel cell system has not been shown till date. In the present case, we have pioneered a way to show the successful integration of COFs into the fuel cell assembly and recorded their proton conducting ability under real operating conditions. It could be observed that the highly porous, solvothermally synthesized **TpBpy-ST** resulted in a fluffily packed pellet causing its easy breakdown on passing of the fuel cell reactant gases *viz.* H₂ and O₂, thereby shorting the fuel cell. On the other hand, the less porous, mechanochemically synthesized **TpBpy-MC** resulted in a more compact pellet that could effectively separate the gases apart, besides showing similar proton conducting behaviour, thereby giving an Open Circuit Potential (OCV) of 0.93 V. The aforementioned phenomena can be attributed to the low porosity of **TpBpy-MC** which effectively inhibits the fuel crossover in PEMFC.

Experimental

Synthesis of **TpBpy-ST** by solvothermal route.

Synthesis of **TpBpy-ST** was achieved solvothermally by reacting 1,3,5-triformylphloroglucinol (**Tp**) (63 mg, 0.3 mmol) and 2,2'-

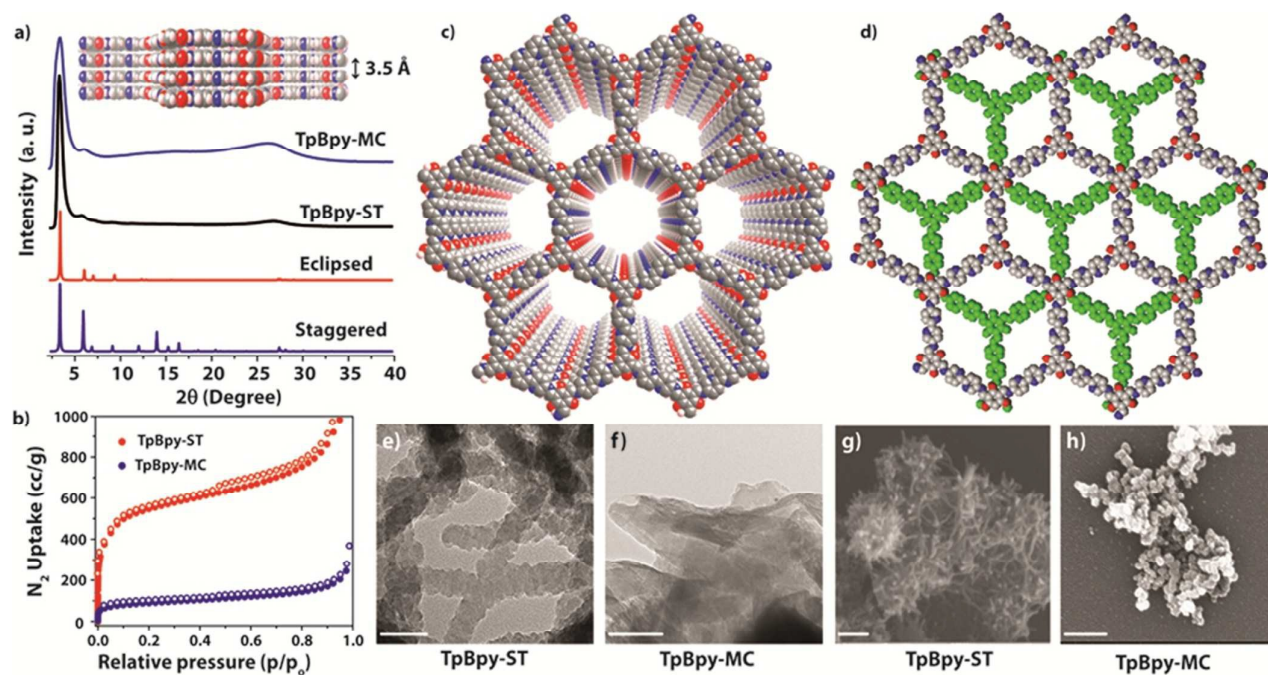


Figure 2. (a) Comparison of the experimental PXRD pattern of **TpBpy-MC** (blue) and **TpBpy-ST** (black) with the simulated eclipsed (red) and staggered (green) forms; insert image showing stacking diagram of **TpBpy**; (b) The N_2 uptake isotherms of **TpBpy-ST** (red) and **TpBpy-MC** (blue); (c) Eclipsed stacking model of **TpBpy**; (d) Staggered stacking model of **TpBpy**; (e) and (f) corresponds to the TEM images of **TpBpy-ST** and **TpBpy-MC** (scale bar represents 100 nm); (g) and (h) SEM images of **TpBpy-ST** and **TpBpy-MC** (scale bar represents 400 nm).

bipyridine-5,5'-diamine (**Bpy**) (83.7 mg, 0.45 mmol) using *N,N*-dimethylacetamide (DMAc) and *o*-dichlorobenzene (*o*-DCB) solvent combination (4.5:1.5 mL) with 0.6 mL of 6 M aqueous acetic acid (AcOH). The reactants were first homogeneously dispersed by ultra sonication for 15 min, degassed through three successive freeze–pump–thaw cycles. Then, the tube was vacuum sealed and heated in an isotherm oven for 72 h at 120 °C. Finally, phase pure material was filtered out and washed with copious amount of DMAc. The collected material was solvent exchanged with DMAc and washed with excess water and acetone. The material was dried under vacuum at 150 °C for 12 h to obtain the as-synthesized **TpBpy-ST** (~79 % isolated yield) (Section S-2, in ESI).

Synthesis of **TpBpy-MC** by mechanochemical route.

A similar compound has also been achieved by employing environmentally benign mechanochemical approach synthesis under ambient conditions, which does not require any special reaction conditions like inert atmosphere, high temperature etc. The starting materials i.e.; **Tp** (63 mg, 0.3 mmol) and **Bpy** (83.7 mg, 0.45 mmol) was initially put into a 5 mL stainless steel jar, with one 7 mm diameter stainless steel ball containing a mixture of 60 μ L of DMAc, 30 μ L of *o*-DCB and 15 μ L of 6M acetic acid. The synthesis was tried at different ball milling time and frequency (Table S1). In the optimised procedure, the reaction mixture was ground for 90 min at 30 Hz, followed by its washing with minimal amount of DMAc and

then with copious amount of water and acetone. The material was dried under vacuum at 150 °C for 12 h to obtain the as-synthesized **TpBpy-MC** (~84 % isolated yield) (Section S-2, in ESI).

Loading experiment of PA to **TpBpy-ST** and **TpBpy-MC**.

The syntheses of **PA@TpBpy-ST** and **PA@TpBpy-MC** were achieved by dipping 300 mg of **TpBpy-ST** or **TpBpy-MC** in 12M H_3PO_4 (50 mL) for 2 h. Afterwards, the materials were filtered and washed with copious amount of water, and finally vacuum dried for 4 h at room temperature.

Results and discussion

The PXRD patterns of **TpBpy-ST** indicate a highly intense peak at $2\theta = 3.6^\circ$ (~ 30000 cps; cps = counts per second) corresponding to the 100 plane reflections (Figure 2a), with minor peaks at 6.0, 6.9, 9.2, 12.1, 12.5, 15.2, and 25.1–28.6°. The π - π stacking distance between the COF layers was calculated as 3.5 Å using d spacing between the (001) planes (25.1–28.6°). A possible 2D structure was generated using Crystal 09 software. The experimental PXRD pattern matches well with the simulated pattern of the eclipsed stacking model (Figure S1). Hence, we propose a structure close to the hexagonal $P6/m$ space group ($a = b = 29.3$ Å, $c = 3.5$ Å, $\alpha = \beta = 90^\circ$, $\gamma = 120^\circ$) for **TpBpy-ST** (Figure S4 and Table S2). An excellent agreement between the experimental and simulated

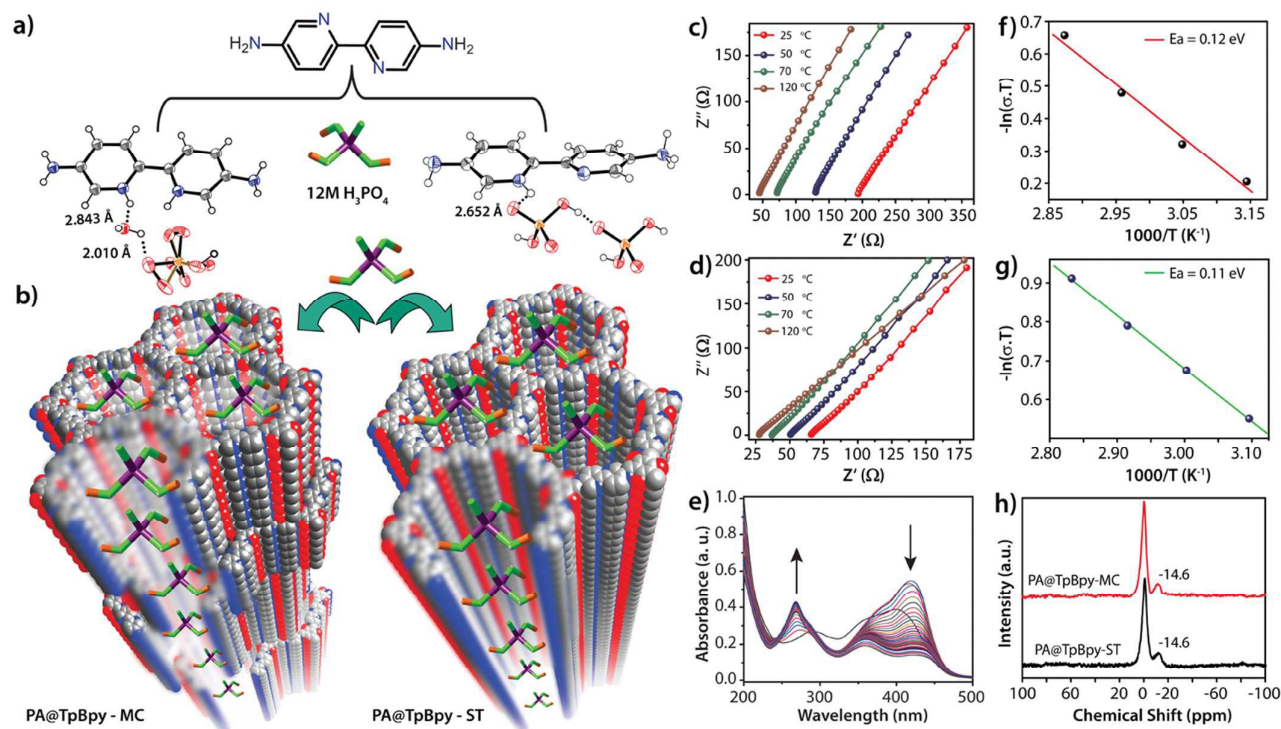


Figure 3. (a) Synthetic scheme of mono protonated bipyridine and doubly protonated bipyridine forms of **PA@Bpy** on loading of 12 M H_3PO_4 ; (b) Synthesis of **PA@TpBpy-ST** or **PA@TpBpy-MC** by loading of 12M H_3PO_4 in **TpBpy-ST** or **TpBpy-MC**; (c, d) corresponds to the variable temperature proton conductivity data of **PA@TpBpy-ST** and **PA@TpBpy-MC**; (e) Changes in the UV-vis spectra of monomer with increasing concentration of H_3PO_4 ; (f, g) Arrhenius plot for **PA@TpBpy-ST** and **PA@TpBpy-MC**; (h) ^{31}P CP-SSNMR of activated **PA@TpBpy-ST** and **PA@TpBpy-MC**.

eclipsed PXRD patterns was confirmed from Pawley refinement ($R_p = 2.5\%$, $R_{wp} = 4.5\%$) (Figure S2). PXRD peak positions of **TpBpy-MC** were found to similar to the **TpBpy-ST**. But the first peak intensity (~ 5000 cps) of the plane (100) is less intense than that of **TpBpy-ST**. This could be attributed to the random displacement of the 2D COF layers due to the constant mechanical force applied during the synthesis. This eventually results into the formation of partially eclipsed structure with poorly distributed accessible pores. As a result of it, the reflections corresponding to the (100) plane get diffused and thus weakens the peak intensity. The broad peak at higher 2θ ($\sim 26^\circ$) is mainly due to the π - π stacking between the COF layers which corresponds to the (001) plane (Figure 2a, S1 and S3).^{8d} The FT-IR peaks of **TpBpy-ST** and **TpBpy-MC** match well with that of the monomer (2E,4E,6E)-2,4,6-tris([(2,2'-bipyridin]-5-yl-amino)methylene)cyclohexane-1,3,5-trione. The FT-IR spectra rule out the presence of minor traces of the starting materials with the disappearance of N-H stretching bands (3112 - 3317 cm^{-1}) of **Bpy** and C=O stretching frequency (1637 cm^{-1}) of **Tp** (Figure S5). In addition, strong peaks corresponding to the stretching frequency of the keto-form was observed at 1607 (C=O) and 1579 (C=C) cm^{-1} , as similar to that of the monomer (Figure S6). The C=O peaks (1609 cm^{-1}) of **TpBpy-ST** get merged with C=C stretching band (1579 cm^{-1}). The ^{13}C CP-MAS solid state NMR of both **TpBpy-ST** and **TpBpy-MC** show carbonyl (C=O) carbon signals at δ 182.8 and 181.5 ppm respectively similar to the (C=O) carbon signal

of the monomer at δ 181.2 ppm (Figure S7). The SEM and TEM images indicate that **TpBpy-ST** crystallizes in an interwoven thread like morphology with aggregation of large number of individual crystallites bearing an average width of 100-300 nm (Figure 2e, 2g, S8 and S10). In contrast, **TpBpy-MC** shows predominant sheet-like morphology with reduced dimensions which is a common characteristic of the mechanochemically delaminated COF crystallites (Figure 2f, 2h, S9 and S11).^{8d,9} Thermogravimetric analysis (TGA) of the activated **TpBpy-ST** and **TpBpy-MC** shows high thermal stability up to 350°C , with a gradual weight loss of 40 and 30% respectively after 360°C due to the decomposition of the respective frameworks (Figure S12 and S13). The permanent porosity of **TpBpy-ST** was evaluated by N_2 adsorption isotherm at 77 K, which shows reversible Type-IV adsorption isotherm. Surface area of the activated COFs calculated using BET model was found to be 1746 and 293 m^2g^{-1} , respectively for **TpBpy-ST** and **TpBpy-MC** (Figure 2b, S14, S16). The decrease in the surface area of **TpBpy-MC** compared to its solvothermal counterpart is presumably due to its sheet-like morphology, unlike the thread like morphology of **TpBpy-ST**. This consequently blocks the long range pore formation in **TpBpy-MC**, rendering N_2 adsorption possible only in the empty accessible pores of the framework. Thus, the diffused stacking peak intensity, as observed from the PXRD spectral study and low surface area of **TpBpy-MC**, as inferred from BET study is a clear reflection of the partial loss in the ordering of the 2D sheets. These COFs

Paper

Journal of Materials Chemistry A

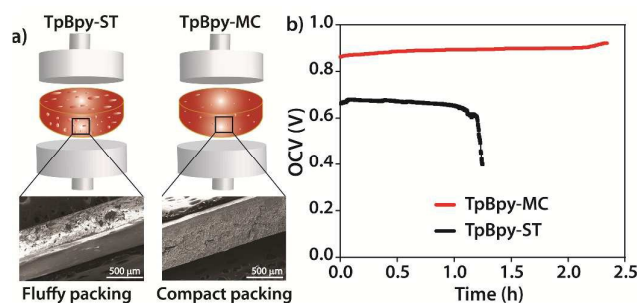


Figure 4. Schematic diagram representing the crystallite ordering in case of (a) PA@TpBpy-ST and PA@TpBpy-MC pellets; (b) Lifetime OCV measurement obtained using PA@TpBpy-ST and PA@TpBpy-MC as solid electrolytes in PEMFC.

show moderate H₂, CO₂ and water uptake (Figure S18 to S22). The pore size distribution of TpBpy-ST and TpBpy-MC shows a narrow pore size distribution between the ranges of 2.1 and 1.4 nm, respectively (Figure S15 and S17).⁹ The chemical stability of TpBpy-ST and TpBpy-MC was evaluated by immersing these COFs in water; strong mineral acids namely 9N HCl, 3M H₃PO₄ and strong base namely 3N NaOH. Interestingly, both COFs remain stable, crystalline and despite such harsh treatment. The FT-IR spectra, PXRD, N₂ adsorption isotherms and SEM of the COFs remain almost unchanged even after 7 days of water and acid treatment. They also exhibit considerable base stability for more than 7 days of treatment with near retention of their molecular crystallinity (Figure S23 to S27). The observable ~20% loss in the surface area after the base treatment could be mainly attributed to the consequent loss of the intra-molecular H bonding which weakens the framework rigidity and stability. The material stability was further checked with increasing phosphoric acid concentrations. It was found that both TpBpy-ST and TpBpy-MC retained their structural integrity even after treatment with 6M and 12M H₃PO₄ for 7 days each (Figure S28 to S30).

Bipyridine (Bpy) moieties have potential to abstract proton from mineral acids and form corresponding bipyridinium salts.¹² For example, the protonation of 2,2'-bipyridine-5,5'-diamine by phosphoric acid leads to a different protonated state of the bipyridine moiety along with the phosphate counter anions (Figure 3a). Interestingly, we could crystallize and solve the corresponding crystal structures of both the monoprotonated 2,2'-bipyridinium-5-amino-5'-ammonium bis-dihydrogen phosphate species (involving only one pyridine N of the Bpy unit and another with free amine N) as well as doubly protonated Bpy species 2,2'-bipyridinium-5,5'-diamino hydrogen phosphate monohydrate (involving both the pyridinic N) (Figure S31 and S32). The degree of protonation of the Bpy unit has been evaluated by dissolving 2,2'-bipyridine-5,5'-diamine in aqueous H₃PO₄ followed by crystallization via slow evaporation of the mother liquor. The mono-protonated structure consists of intramolecular hydrogen bonding between the protonated pyridine unit and the dihydrogen phosphate [H₂PO₄⁻] moieties [N-H...O9; D = 2.816(2) Å, d =

2.023(2) Å, $\theta = 153.5^\circ$] (Table S3), that are hydrogen bonded among themselves [O-H...O; 2.652(3) Å, 1.844(2) Å, 160.7°]. On the other hand, the doubly protonated species includes hydrogen bonded water molecules [N-H...O; 2.843(3) Å, 2.010(4) Å, 159.5°] within the crystal structure, which connects the protonated pyridinic N and monohydrogen phosphate [HPO₄²⁻] [O-H...O; 2.701(5) Å, 1.884(4) Å, 153.5°] (Table S4). The protonation of the Bpy monomer by H₃PO₄ can also be well correlated with the changes in the solution state UV spectra (increasing intensity of peak at 270 nm and diminished intensity of the peak at 418 nm) (Figure 3e and S33). This lays a strong foundation for easy modulation and evaluation of the protonation step. Furthermore, the protonation at the primary amine site is less likely due to unavailability of the same in the plain COF backbone. The ³¹P CP-SSNMR solid state NMR of both activated PA@TpBpy-ST and PA@TpBpy-MC shows two distinctive signals at δ 0.0 and -14.6 ppm. The peak at δ 0.0 ppm is due to the orthophosphoric acid (H₃PO₄) and δ -14.6 ppm is assigned to the condensation products of phosphoric acid, may be dimer or oligomers.^{13a,b} It is worthy to note that, unlike the activated samples, the ³¹P CP-SSNMR spectra of the non-activated ones shows only one signal at 0.0 ppm, corresponding to the loaded H₃PO₄ (Figure S35), thereby indicating the condensation of the phosphoric acid on thermal activation. Such loaded species have close resemblance with the H₃PO₄ doped polybenzimidazole (PBI) membranes, (H₃PO₄@PBI)¹³, one of the currently employed benchmark high temperature solid state electrolytes in PEMFCs. We envisage that both the mono protonated as well as the doubly protonated species will prevail within the TpBpy COF backbone upon H₃PO₄ loading, which strongly motivated us to perform the loading experiment involving both TpBpy-ST and TpBpy-MC. In solid state COFs, proton conductivity is defined by $\sigma = \sum n.q.\mu$; where n, q and μ are the number, charge and mobility of the carrier molecules, respectively. H₃PO₄ has high proton concentration, low volatility (>158 °C), high mobility and conductivity (ca. 10⁻¹ Scm⁻¹). The H₃PO₄ loading in TpBpy-ST and TpBpy-MC was achieved by simply immersing the evacuated COF materials in 12M H₃PO₄ for 2 h. Further washing with copious amount of water (100 mL x2) followed by overnight activation at 353K under dynamic vacuum lead to H₃PO₄ loaded TpBpy-ST and TpBpy-MC, henceforth denoted as PA@TpBpy-ST and PA@TpBpy-MC, respectively. It is noteworthy that the PXRD, FT-IR and ¹³C SSNMR spectra of the COF samples filtered from the 12M H₃PO₄ solutions show all the characteristic peaks of the parent COFs with certain degree of broadening (Figure S36 to S43), which demonstrate the architectural stability of the COF backbone. During this treatment, the COF pores get eventually filled by the incoming guest molecules. This in turn reduces the exposure of the 100 planes for X-ray diffraction thereby decreasing the corresponding peak intensity after acid treatment. The H₃PO₄ loading phenomenon is in accordance with the partial decrease in porosity as measured from N₂ adsorption isotherm studies (80 m²g⁻¹), which alludes to the fact that the H₃PO₄

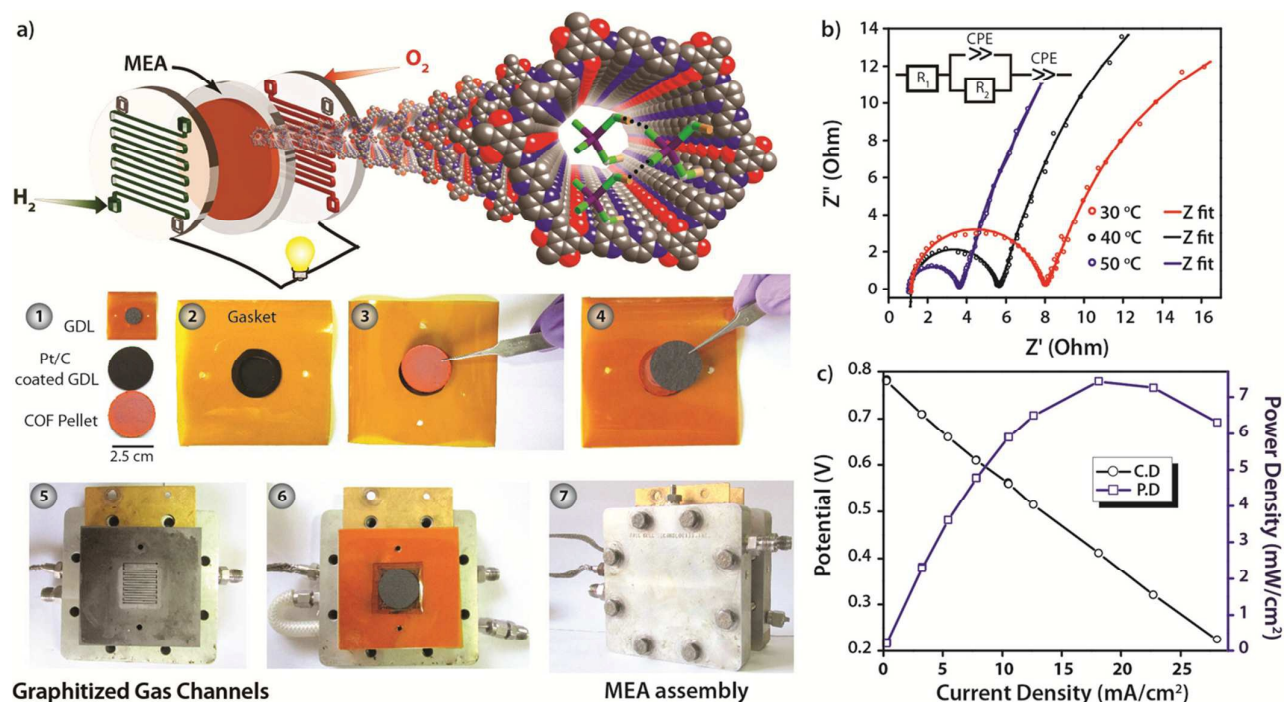


Figure 5. (a) Schematic representation of MEA making using pelletized COF powder (1) Preparation of Pt coated GDL (as anode and cathode), COF pellet (as solid electrolyte), (2-4) Sandwiching of COF pellet between two electrodes; (5-7) Assembly of the MEA into a single cell stack; (b) Nyquist plots obtained at different temperatures (in °C), evidencing the high proton conducting ability of the material ($1.4 \times 10^{-2} \text{ S cm}^{-1}$ at 50 °C); (c) Fuel cell polarization plot obtained at 50°C using dry H₂, Pt, C/ COF pellet/Pt, C, dry O₂ electrochemical cell

predominantly blocks the pores of the framework during the course of its loading in both **TpBpy-ST** and **TpBpy-MC**. The decrease in porosity upon 12 M H₃PO₄ doping may be advantageous to overcome hydrogen fuel crossover, while high stability with retention of intrinsic properties ensure its sustainability in fuel cell operating conditions as discussed later on. Interestingly, **TpBpy-ST** shows greater weight loss step (~15 wt %) than **TpBpy-MC** (~11 wt %), justified from the fact that the former has higher porosity which could therefore accommodate more water and acid molecules comparatively. The reproducibility of the acid loading was confirmed by TGA study on multiple batches (Figure S12 and S13). In order to validate the concept of phosphoric acid loading, we tried to evacuate the loaded H₃PO₄ molecules out of the **PA@TpBpy-ST** pores. As expected the 100-plane intensity increased while the 001 plane intensity decreased on evacuating the H₃PO₄ molecules out of its pores. Interestingly the surface area increased up to 750 m²/g. However, complete restoration of the framework porosity cannot be expected due to the polymerization of phosphoric acid units within the COF framework.

The proton conductivities of **TpBpy-ST**, **TpBpy-MC**, **PA@TpBpy-ST** and **PA@TpBpy-MC** were measured by quasi-four-probe method, using the Solartron 1286 Electrochemical Interface equipped with Frequency Response Analyser. The conductivities were determined from the semicircles in the Nyquist plots, wherein the high frequency intercept can be ascribed to the bulk resistance generated from the materials.

As expected, both **TpBpy-ST** and **TpBpy-MC** as such do not exhibit any notable proton conduction which signifies that the parent COF backbones act as mere support and are devoid of any proton carriers. Temperature dependent proton conducting ability of **PA@TpBpy-ST** and **PA@TpBpy-MC** were studied from 233 to 393 K. The conductivity was found to improve with increase in temperature (Figure 3c, 3d and S44). A maximum proton conductivity of 1.98×10^{-3} and $2.5 \times 10^{-3} \text{ S cm}^{-1}$ was measured at 393 K for **PA@TpBpy-ST** and **PA@TpBpy-MC** respectively (Figure. 3c and 3d). The proton conductivity of **PA@TpBpy-ST** is comparable with its MOF counterparts i.e. **PA@MIL-101** ($1.3 \times 10^{-3} \text{ S cm}^{-1}$ at 120 °C 0% RH),¹⁴ while being two orders of magnitude higher than the previously reported **PA@Tp-Azo** ($6.7 \times 10^{-5} \text{ S cm}^{-1}$ at 120 °C, 0% RH),¹¹ which we believe to the best of our knowledge, is the only COF evidenced as a proton conductor till date. It is to be noted that the values are higher than the recently reported imidazole impregnated porous organic polymer, **Im@Td-PNDI 1** ($9.04 \times 10^{-5} \text{ S cm}^{-1}$) and **Im@Td-PPI 2** ($3.49 \times 10^{-4} \text{ S cm}^{-1}$).¹⁵ The activation energy value were calculated to be 0.12 and 0.11 eV for **PA@TpBpy-ST** and **PA@TpBpy-MC**, respectively (Figure S45), that is similar to the previously reported **PA@TpAzo** (0.11 eV) indicating Grotthuss proton hopping mechanism operating in both cases.¹⁶ Clearly, as evident from the preliminary studies, both **PA@TpBpy-ST** and **PA@TpBpy-MC** show almost similar proton conductivity ability under similar conditions although they could be observed to differ in terms of the morphology, surface area and the degree of

crystallinity. However, they are similar in terms of their chemical structure and composition (as confirmed from their PXRD peak positions, FT-IR spectra and solid state NMR spectra). Both **TpBpy-ST** and **TpBpy-MC** have bipyridine units in their backbone that are equally capable of immobilizing the phosphoric acid (PA) moieties via hydrogen bonding on their acidification (as evident from the crystal structure of Bpy- H_2PO_4). Conspicuous by this structural similarity and comparable activation energy, we believe that the proton hopping possibly occurs by the structural diffusion of protons *via* phosphoric units, hydrogen bonded to the bipyridine site in both **PA@TpBpy-ST** and **PA@TpBpy-MC**. Thus we believe that this structural similarity confers similar proton conducting ability to both **PA@TpBpy-ST** and **PA@TpBpy-MC**.

Encouraged by the high proton conductivity of **TpBpy** COFs, we have validated the concept of utilizing such materials as solid-state electrolytes for PEFMCs in H_2/O_2 fuel cell operating conditions (Figure 5 and S46). Initially ~ 250 mg of **PA@TpBpy-ST** powder was pressed into pellets of thickness (~ 850 μm) and sandwiched between two Pt-C gas diffusion electrodes (loading of 1 mg Pt cm^{-2}) to fabricate a 2×2 cm^2 MEA (Membrane Electrode Assembly), performed using standard PEFMC protocol.¹⁷ D.C. measurements were carried out on the assembled MEA using dry H_2 and O_2 gases as reactants that were passed into the fuel cell assembly at a controlled flow rate (25-30 sccm). A preliminary test carried out to optimize the flow rate of the reactant gases H_2 and O_2 indicated that, although the OCV initially increased on increasing the flow rate (up to a maximum of 80 sccm), the OCV lifetime was detrimentally affected, due to the mechanical breakdown of the pellet thereafter. Thus the lifetime test of OCV was performed at 50 sccm at both the anode and cathode in order to maximize the OCV lifetime (Figure S52). The MEA fabricated using the solvothermally synthesized COF pellets **PA@TpBpy-ST** showed a starting OCV of 0.66 ± 0.02 V at 50 $^\circ\text{C}$. However, the OCV was constant for ~ 1.2 h and began to drop thereafter. To check the reproducibility, a new MEA was fabricated using a different **PA@TpBpy-ST** pellet (of a different batch). Interestingly, the OCV was found to be very close to that of the first one (i.e. 0.67 ± 0.02 V at 50 $^\circ\text{C}$), which continued remaining stable up to ~ 1.2 h before decreasing abruptly to ~ 0.30 V after that (Figure S49). On the other hand, the MEA fabricated using mechanochemically synthesized **PA@TpBpy-MC** pellets showed a satisfying OCV of 0.86 ± 0.02 V at 30 $^\circ\text{C}$ that increased to a maximum of 0.90 V, stable for about 2.5 h on further increasing the temperature to 50 $^\circ\text{C}$, on thermal activation of the Pt catalyst (Figure 4b and S47). For better clarity, SEM imaging of the pellets used for the proton conduction were performed. The cross section of the COF pellets indicated compact packing of the material in case of mechanically synthesized **PA@TpBpy-MC** and coarse nature in case of solvothermally synthesized **PA@TpBpy-ST** pellets (Figure 4 and Figure S50). The PXRD and IR of the used-pellet matched very well with the fresh sample (**PA@TpBpy-ST** and **PA@TpBpy-MC**), which confirmed the chemical intactness of

the material (Figure S51). Thus the drastic drop in the OCV in case of solvothermally synthesized COF pellets could be attributed to the detrimental effect of the highly porous nature of the material that resulted in an easy mechanical breakdown of the pellet. This facilitated an easy fuel crossover across the pellet separating the two Pt electrodes, in turn shorting the fuel cell circuit. The concentration of H_2 gas at the cathode, resulting from the fuel leak was evaluated by studying the *in situ* Linear Sweep Voltammogram (LSV) profile of the **PA@TpBpy-ST** constituted single cell (Figure S48). The potential of the cathode was then linearly scanned from its Open Circuit Voltage (which was about 0.10 V) at a scan rate of 2 mV s^{-1} upto 0.5 V, such that the hydrogen molecules that have possibly diffused across the cathode are instantly oxidized under mass transfer limited conditions. The cell was found to exhibit a mass transfer limited current density (J_{lim}) of 8 mA cm^{-2} at 50 $^\circ\text{C}$ and the H_2 cross over flux at cathode was calculated to be 4.1×10^{-8} $\text{mol cm}^{-2} \text{s}^{-1}$ at 50 $^\circ\text{C}$.

Along with the electromotive force (emf) measurements, the effect of temperature on the fuel cell reaction was studied using *in situ* impedance technique at a frequency range of 1 MHz– 100 Hz and 10 mV voltage amplitude. The high frequency resistance revealed a solid-state electrolyte conductivity of 1.4×10^{-2} S cm^{-1} with a distinct catalyst charge transfer resistance (R_2) at the low frequency region (Figure 5b and S53). The improvement in the solid-state electrolyte conductivity in the real fuel cell conditions over the quasi-four probe conductivity could be attributed to the improved contact at the electrode-electrolyte interface. On further increase in temperature, owing to the thermal activation of the catalyst, R_2 was found to decrease while the solid-state electrolyte resistance remained largely unaffected. Employing COFs as PEFMC solid electrolytes for the first time, fuel cell reaction was driven by polarizing the fuel cell. The OCV lifetime measurement test of the MEA fabricated using **PA@TpBpy-MC** pellet revealed that the pellet could effectively separate reactants gases only till 50 $^\circ\text{C}$. As the ultimate fuel cell performance of the pellet is decided by not just the proton conducting ability of the pellet, but also its gas separating ability, which is very essential to build a stable OCV, the operating temperature was limited to 50 $^\circ\text{C}$. Considering the large thickness of our solid electrolyte, the flow rate of the reactant gases was increased just before polarizing the cell in order to prevent fuel starvation of MEA under this stress. This resulted in slight increase in the OCV from 0.9 to 0.92 V after which the polarization of MEA was initiated. The current (I)-voltage (V) polarization plots revealed a maximum current density of 29 mA cm^{-2} and maximum power density of 7 mW cm^{-2} , thereby ascertaining the completion of the cell circuit and proton conducting nature of the COF (Figure 5c). Although the performance is less compared to the Nafion[®] based PEMFC, we believe that this is a direct effect of the huge disparity in the electrolyte thickness in both the cases (50 μm in Nafion vs. 900 μm in COFs), as the rest of the conditions are similar.

Conclusions

In summary, we for the first time could introduce covalent organic frameworks as proton conducting solid electrolytes in fuel cells. We have prepared bipyridine functionalized covalent organic frameworks (**TpBpy**) using solvothermal as well as simple mechanochemical route. These COFs exhibit permanent porosity, crystallinity and strong acid-base stability. We have then loaded mineral acid viz. H_3PO_4 inside the framework backbones. Interestingly, these COFs retain their crystallinity and stability that made them attractive for proton conduction applications. While the parent COFs exhibit negligible conductivity, the H_3PO_4 loaded COFs i.e. the **PA@TpBpy-ST** and **PA@TpBpy-MC** show decent proton conductivity. Moreover, the less porous nature of **PA@TpBpy-MC** has been successfully leveraged to obtain a stable OCV and a solid-state electrolyte conductivity of $1.4 \times 10^{-2} \text{ Scm}^{-1}$ while the solvothermally synthesized material proves ineffective under similar conditions. Thus, for the first time we have successfully leveraged such characteristics of mechanochemically synthesized COF to showcase their advantage over solvothermal counterparts. We believe that this demonstration will unravel further avenues for the use of mechanochemically synthesized COFs for applications involving acute conditions such as solid electrolytes in fuel cells.

Acknowledgements

D.B.S acknowledges CSIR for postdoctoral Nehru research fellowship. M.B, S.K and T.K acknowledge CSIR and H.B.A, B.P.B, and B.G acknowledge UGC, India for research fellowship. R.B and K.S acknowledge CSIR's XIIth Five Year Plan Project (CSC0122 and CSC0102) for funding. Financial assistance from DST (SB/S1/IC-32/2013) is acknowledged. We acknowledge Dr. T. G. Ajithkumar, Shrikant M. Kunjir and Anjali Krishna M. for the NMR facility; Dr. C. Ramesh and Dr. Guruswamy K. for the PXRD facility.

Notes and references

- a) K. Tanaka, Wiley-VCH, Weinheim (2003); b) S. L. James, C. J. Adams, C. Bolm, D. Braga, P. Collier, T. Friščić, F. Grepioni, K. D. M. Harris, G. Hyett, W. Jones, A. Krebs, J. Mack, L. Maini, A. G. Orpen, I. P. Parkin, W. C. Shearouse, J. W. Steed and D. C. Waddell, *Chem. Soc. Rev.*, 2012, **41**, 413-447.
- a) L. R. MacGillivray, J. L. Reid and J. A. Ripmeester, *J. Am. Chem. Soc.*, 2000, **122**, 7817-7818; b) T. Friščić, *Chem. Soc. Rev.*, 2012, **41**, 3493-3510.
- a) M. K. Beyer and H. Clausen-Schaumann, *Chem. Rev.*, 2005, **105**, 2921-2948; b) R. E. Morris and S. L. James, *Angew. Chem. Int. Ed.*, 2013, **52**, 2163-2165.
- a) T. Friščić, D. G. Reid, I. Halasz, R. S. Stein, R. E. Dinnebier and M. J. Duer, *Angew. Chem. Int. Ed.*, 2010, **49**, 712-715; b) T. Friščić and L. R. MacGillivray, *Chem. Commun.*, 2003, **11**, 1306-1307; c) K. Tanaka and F. Toda, *Chem. Rev.*, 2000, **100**, 1025-1074; d) T. Friščić, I. Halasz, P. J. Beldon, A. M. Belenguer, F. Adams, S. A. J. Kimber, V. Honkimäki and R. E. Dinnebier, *Nat. Chem.*, 2013, **5**, 66-73.

- a) A. P. Côté, A. I. Benin, N. W. Ockwig, M. O'Keeffe, A. J. Matzger and O. M. Yaghi, *Science*, 2005, **310**, 1166-1170; b) X. Feng, X. Ding and D. Jiang, *Chem. Soc. Rev.*, 2012, **41**, 6010-6022; c) C. J. Doonan, D. J. Tranchemontagne, T. G. Glover, J. R. Hunt and O. M. Yaghi, *Nat. Chem.*, 2010, **2**, 235-238; d) Y. Zeng, R. Zou, Z. Luo, H. Zhang, X. Yao, X. Ma, R. Zou and Y. Zhao, *J. Am. Chem. Soc.*, 2015, **137**, 1020-1023; e) D. D. Medina, J. M. Rotter, Y. Hu, M. Dogru, V. Werner, F. Auras, J. T. Markiewicz, P. Knochel and T. Bein, *J. Am. Chem. Soc.*, 2015, **137**, 1016-1019; f) S. Kandambeth, V. Venkatesh, D. B. Shinde, S. Kumari, A. Halder, S. Verma and R. Banerjee, *Nat. Commun.*, doi:10.1038/ncomms7786 (2015).
- a) H. Furukawa and O. M. Yaghi, *J. Am. Chem. Soc.*, 2009, **131**, 8875-8883; b) Y. -B. Zhang, J. Su, H. Furukawa, Y. Yun, F. Gándara, A. Duong, X. Zou and O. M. Yaghi, *J. Am. Chem. Soc.*, 2013, **135**, 16336-16339; c) M. G. Rabbani, A. K. Sekizkardes, Z. Kahveci, T. E. Reich, R. Ding and H. M. El-Kaderi, *Chem. Eur. J.*, 2013, **19**, 3324-3328; d) K. T. Jackson, T. E. Reich and H. M. El-Kaderi, *Chem. Commun.*, 2012, **48**, 8823-8825; e) S. Kandambeth, D. B. Shinde, M. K. Panda, B. Lukose, T. Heine and R. Banerjee, *Angew. Chem. Int. Ed.* 2013, **52**, 13052-13056; f) M. Dogru, A. Sonnaier, A. Gavryushin, P. Knochel and T. Bein, *Chem. Commun.*, 2011, **47**, 1707-1709; g) S. -Y. Ding, J. Gao, Q. Wang, Y. Zhang, W. -G. Song, C. -Y. Su and W. Wang, *J. Am. Chem. Soc.*, 2011, **133**, 19816-19822; h) Q. Fang, S. Gu, J. Zheng, Z. Zhuang, S. Qiu and Y. Yan, *Angew. Chem. Int. Ed.* 2014, **53**, 2878-2882; i) D. B. Shinde, S. Kandambeth, P. Pachfule, R. R. Kumar and R. Banerjee, *Chem. Commun.*, 2015, **51**, 310-313; j) S. Wan, J. Guo, J. Kim, H. Ihee and D. Jiang, *Angew. Chem. Int. Ed.*, 2008, **47**, 8826-8830; k) S. Dalapati, S. Jin, J. Gao, Y. Xu, A. Nagai and D. Jiang, *J. Am. Chem. Soc.*, 2013, **135**, 17310-17313; l) C. R. DeBlase, K. E. Silberstein, T. -T. Truong, H. D. Abruña and W. R. Dichtel, *J. Am. Chem. Soc.*, 2013, **135**, 16821-16824; m) S. Wan, F. Gándara, A. Asano, H. Furukawa, A. Saeki, S. K. Dey, L. Liao, M. W. Ambrogio, Y. Y. Botros, X. Duan, S. Seki, J. F. Stoddart and O. M. Yaghi, *Chem. Mater.*, 2011, **23**, 4094-4097; n) H. Xu, J. Gao and D. Jiang, *Nat. Chem.*, 2015, **7**, 905-912; o) N. Huang, X. Ding, J. Kim, H. Ihee and D. Jiang, *Angew. Chem. Int. Ed.*, 2015, **54**, 8704-8707.
- a) N. Stock and S. Biswas, *Chem. Rev.*, 2012, **112**, 933-969; b) M. Eddaoudi, D. F. Sava, J. F. Eubank, K. Adil and V. Guillerme, *Chem. Soc. Rev.*, 2015, **44**, 228-249; c) A. Carné-Sánchez, I. Imaz, M. Cano-Sarabia and D. Maspoch, *Nat. Chem.*, 2013, **5**, 203-211; d) D. D. Medina, J. M. Rotter, Y. Hu, M. Dogru, V. Werner, F. Auras, J. T. Markiewicz, P. Knochel and T. Bein, *J. Am. Chem. Soc.*, 2015, **137**, 1016-1019.
- a) B. Icli, N. Christinat, J. Tönnemann, C. Schüttler, R. Scopelliti and K. Severin, *J. Am. Chem. Soc.*, 2009, **131**, 3154-3155; b) A. Orita, L. Jiang, T. Nakano, N. Ma and J. Otera, *Chem. Commun.*, 2002, 1362-1363; c) J. Huang, J. A. Moore, J. H. Acquaye and R. B. Kaner, *Macromolecules*, 2005, **38**, 317-321; d) S. Chandra, S. Kandambeth, B. P. Biswal, B. Lukose, S. M. Kunjir, M. Chaudhary, R. Babarao, T. Heine and R. Banerjee, *J. Am. Chem. Soc.*, 2013, **135**, 17853-17861.
- a) B. P. Biswal, S. Chandra, S. Kandambeth, B. Lukose, T. Heine and R. Banerjee, *J. Am. Chem. Soc.*, 2013, **135**, 5328-5331; b) G. Das, D. B. Shinde, S. Kandambeth, B. P. Biswal and R. Banerjee, *Chem. Commun.*, 2014, **50**, 12615-12618.
- a) K. -D. Kreuer, S. J. Paddison, E. Spohr and M. Schuster, *Chem. Rev.*, 2004, **104**, 4637-4678; b) J. A. Hurd, R. Vaidhyanathan, V. Thangadurai, C. I. Ratcliffe, I. L. Moudrakovski, G. K. H. Shimizu, *Nat. Chem.*, 2009, **1**, 705-710; c) S. Bureekaew, S. Horike, M. Higuchi, M. Mizuno, T. Kawamura, D. Tanaka, N. Yanai and S. Kitagawa, *Nat. Mater.*, 2009, **8**, 831-836; d) K. A. Mauritz and R. B. Moore, *Chem. Rev.*, 2004, **104**, 4535-4585; e) M. Yoon, K. Suh, H. Kim, Y. Kim, N. Selvapalam and K. Kim, *Angew. Chem. Int. Ed.*, 2011,

- 50, 7870-7873; f) T. Yamada, M. Sadakiyo and H. Kitagawa, *J. Am. Chem. Soc.*, 2009, **131**, 3144-3145; g) M. Yoon, K. Suh, S. Natarajan and K. Kim, *Angew. Chem. Int. Ed.*, 2013, **52**, 2688-2700; h) D. Umeyama, S. Horike, M. Inukai, T. Itakura and S. Kitagawa, *J. Am. Chem. Soc.*, 2012, **134**, 12780-12785; i) M. R. Karim, K. Hatakeyama, T. Matsui, H. Takehira, T. Taniguchi, M. Koinuma, Y. Matsumoto, T. Akutagawa, T. Nakamura, S. -i. Noro, T. Yamada, H. Kitagawa and S. Hayami, *J. Am. Chem. Soc.*, 2013, **135**, 8097-8100; j) S. Horike, D. Umeyama and S. Kitagawa, *Acc. Chem. Res.*, 2013, **46**, 2376-2384; k) P. Ramaswamy, N. E. Wonga and G. K. H. Shimizu, *Chem. Soc. Rev.*, 2014, **43**, 5913-5932; l) S. -L. Lia and Q. Xu, *Energy Environ. Sci.*, 2013, **6**, 1656-1683; m) S. Horike, Y. Kamitsubo, M. Inukai, T. Fukushima, D. Umeyama, T. Itakura and S. Kitagawa, *J. Am. Chem. Soc.*, 2013, **135**, 4612-4615.
- 11 S. Chandra, T. Kundu, S. Kandambeth, R. BabaRao, Y. Marathe, S. M. Kunjir and R. Banerjee, *J. Am. Chem. Soc.*, 2014, **136**, 6570-6573.
- 12 a) J. Zaccaro, M. Bagieu-Beucher, A. Ibanez and R. Masse, *J. Solid State Chem.*, 1996, **124**, 8-16; b) J. Oueslati, A. Oueslati, C. Ben Nasr and F. Lefebvre, *Solid State Sci.*, 2006, **8**, 1067-1073.
- 13 a) I. Nicotera, V. Kosma, C. Simari, S. Angioni, P. Mustarelli and E. Quartarone, *J. Phys. Chem. C*, 2015, **119**, 9745-9753; b) S. Suarez, N. K. A. C. Kodiweera, P. Stallworth, S. Yu, S. G. Greenbaum and B. C. Benicewicz, *J. Phys. Chem. B*, 2012, **116**, 12545-12551; c) E. Quartarone and P. Mustarelli, *Energy Environ. Sci.*, 2012, **5**, 6436-6444; d) O. E. Kongstein, T. Berning, B. Børresen, F. Seland and R. Tunold, *Energy*, 2007, **32**, 418-422; e) D. Mecerreyes, H. Grande, O. Miguel, E. Ochoteco, R. Marcilla and I. Cantero, *Chem. Mater.*, 2004, **16**, 604-607.
- 14 V. G. Ponomareva, K. A. Kovalenko, A. P. Chupakhin, D. N. Dybtsev, E. S. Shutova and V. P. Fedin, *J. Am. Chem. Soc.*, 2012, **134**, 15640-15643.
- 15 Y. Ye, L. Zhang, Q. Peng, G. -E. Wang, Y. Shen, Z. Li, L. Wang, X. Ma, Q. -H. Chen, Z. Zhang and S. Xiang, *J. Am. Chem. Soc.*, 2015, **137**, 913-918.
- 16 N. Agmon, *Chem. Phys. Lett.*, 1995, **244**, 456-462.
- 17 a) H. B. Aiyappa, S. Saha, P. Wadge, R. Banerjee and S. Kurungot, *Chem. Sci.*, 2015, **6**, 603-607. b) The conventional Nafion® membrane used for PEFMC has a maximum thickness of 50 µm, while the thickness of the pellet used for the MEA making in the present study is about 950 µm. This 19-20 times increase in the pellet thickness undoubtedly adds to the overall cell resistance besides increasing the through-plane proton diffusion path towards the catalyst, which directly reflects in the power density of the system (as Power Density= Current Density × Voltage). Thus we believe that if a COF membrane could be used in place of the pellet, a power density very close to that of the state of art PEMFCs could be achieved. However presently, the membrane processability of COFs is a challenge owing to their highly insoluble form.

Table of Contents

